Solar Photovoltaic Dispatch Margins with Stochastic Unbalanced Demand in Distribution Networks

M. Ramin Feizi[a,*], Shengfei Yin[a] and Mohammad E. Khodayar[a]

[a]Department of Electrical and Computer Engineering, Southern Methodist University, Dallas, TX, United States

ARTICLE INFO

Keywords:
photovoltaic dispatch margin, unbalanced distribution system, uncertainty

ABSTRACT

The increase in the generation capacity of the variable photovoltaic units introduces new challenges to the operation of the unbalanced three-phase distribution networks. In this paper, a two-stage optimization problem is formulated to identify the feasible dispatch margins of photovoltaic generation considering the distribution network operation constraints. The proposed problem is solved using the column-and-constraint generation approach. The distribution network constraints are formulated as second-order cone constraints. The uncertainty in the forecasted demand and maximum photovoltaic generation as well as the unbalanced operation of the distribution network is considered in the proposed approach. The dispatch margins of photovoltaic generation are quantified considering the worst-case realization of demand in the distribution network. The impacts of energy storage and the ramping limits of the dispatchable generation resources on the dispatch margins of photovoltaic generation are addressed in this network. The dispatch margins of photovoltaic generation are quantified in the modified IEEE 13-bus system. It is shown that enforcing the ramping rates for the dispatchable units will increase the lower dispatch margins of photovoltaic generation, and leveraging energy storage increases the difference between the lower and upper photovoltaic dispatch margins.

1. Introduction

Driven by regulatory policies, renewable portfolio standards, and federal tax credits, the capacity of solar power generation is increasing in the transmission and distribution sectors [1]. Solar power generation, the fastest growing technology among other renewable energy resources in the distribution networks, is expected to increase to 8.3 trillion kWh by 2050 worldwide as the manufacturing costs decrease. Such generation capacity will represent 70% of the total renewable generation and serves up to 16% of the electric demand worldwide [2].

Recent studies were focused on various approaches to enhance the capacity of solar photovoltaic (PV) generation in transmission and distribution networks [3, 4, 5]. In [3] the hosting capacity of rooftop PV generation is quantified using Monte Carlo simulation. The impacts of the number of PV installations and their power factors, the loading of the feeders and the conductor characteristics on the PV hosting capacity were investigated. A voltage profile design algorithm is proposed in [4] to handle the variation of the demand profile and improve the hosting capacity of the PV generation in the distribution feeders. In [5] a mixed-integer nonlinear programming (MINLP) problem is formulated to maximize the PV hosting capacity by controlling the voltage regulators, PV inverters, capacitor banks as well as controllable branch switches. The power flow problem is solved using the OpenDSS simulator and the formulated MINLP problem is solved using genetic algorithm. In [6] a Nomogram-based approach is proposed to quantify the hosting capacity of low voltage distribution systems and determine the connection criteria for PV generation units. The energy storage operation set points are determined to tackle the overvoltage challenges in the distribution network with high penetration of PV generation in [7]. The PV hosting capacity is increased in [8] by providing voltage droop control in active transformers. A Monte Carlo-based framework is proposed in [9] to quantify the hosting capacity of PV generation in distribution feeder and the sensitivity of PV hosting capacity to the circuit characteristics is evaluated.

The expansion planning of static VAR compensators was proposed as a two-stage stochastic programming problem in [10] to increase the installed capacity of PV generation in distribution networks. Here, the Benders decomposition technique was used to solve the formulated problem. An integrated generation and transmission expansion planning framework is proposed in [11] to maximize the large-scale solar PV penetration and minimize the investment on the

⋆This document is the results of the research project funded by the National Science Foundation Grant ECCS-1710923.

*Corresponding author

mfeizi@smu.edu (M. Ramin Feizi); gyin@smu.edu (Shengfei Yin); mkhodayar@smu.edu (Mohammad E. Khodayar)

ORCID(s): 0000-0002-7270-6518 (M. Ramin Feizi)

Nomenclature

Parameters

$\boldsymbol{p}_l$	Vector of binary parameters representing the availability of phases in a distribution branch
$\boldsymbol{r}_l$	Resistance matrix of a distribution branch
$\boldsymbol{x}_l$	Inductive reactance matrix of a distribution branch
Γ_t^{φ}	The budget of uncertainty for real and reactive power
$\mathbf{AD}$	Bus-demand incidence matrix
$\mathbf{AE}$	Bus-energy storage incidence matrix
$\mathbf{AG}$	Bus-distributed generation incidence matrix
$\mathbf{AI}$	Bus-branch incidence matrix for buses at the receiving end of the branches
$\mathbf{AL}$	Bus-branch incidence matrix
$\mathbf{AN}$	Bus-feeder incidence matrix
$\mathbf{AV}$	Bus-photovoltaic incidence matrix
$\mathbf{BF}$	Bus-branch incidence matrix for buses at the sending end of the branches
$\mathbf{BN}$	Feeder-bus incidence matrix
$\mathbf{LN}$	Feeder-branch incidence matrix
$\overline{\mathbf{I}}_l$	Vector of square of current magnitude's upper limits
$\underline{\mathbf{V}}_b, \overline{\mathbf{V}}_b$	Vector of square of voltage magnitude's lower and upper limits
$\underline{P}_{d,t}^{\varphi}, \overline{P}_{d,t}^{\varphi}$	Lower and upper bounds of uncertain real power demand
$\underline{Q}_{d,t}^{\varphi}, \overline{Q}_{d,t}^{\varphi}$	Lower and upper bounds of uncertain reactive power demand
$C_e^{0,\varphi}$	The initial energy of an energy storage unit
$P_{(.)}^{\varphi,max}$	Real power capacity of a unit
$P_{d,t}^{\varphi,f}$	Forecasted real power demand
$P_{v,t}^{\varphi,f,m}$	Forecasted maximum PV generation
$P_v^{\varphi,max}$	Capacity of a PV generation unit
PF_n	Power factor at distribution feeder
$Q_{(.)}^{\varphi,max}$	Reactive power capacity of a unit
$Q_{d,t}^{\varphi,f}$	Forecasted reactive power demand
$S_{(.)}^{\varphi,max}$	Maximum apparent power of a unit
$SL_l^{\varphi,max}$	Apparent power capacity of a distribution branch

Sets and Indecies

$\mathcal{B}$	Set of buses
$\mathcal{S}$	Set of scenarios
b	Index of bus
d	Index of demand
e	Index of energy storage
i	Index of distributed generation
l	Index of distribution branch
m	Index of scenario
n	Index of distribution feeder
v	Index of PV generation

Variables

$\mathbf{I}_{l,t}^m$	Vector of square of current magnitudes
$\mathbf{U}_{b,t}^m$	Vector of square of voltage magnitudes
μ	Dual variable
$\rho_{d,t}^{(.),\varphi,m}$	Auxiliary binary variable representing the worst-case realization of demand
$\sigma_{v,t}^{\varphi,m}$	Auxiliary binary variables representing the worst-case realization of PV generation
$\tilde{l}_{v,t}^{\varphi}$	Risk-based lower margin of PV dispatch
$\tilde{u}_{v,t}^{\varphi}$	Risk-base upper margin of PV dispatch
$C_{e,t}^{\varphi,m}$	Available energy in the energy storage unit
$l_{v,t}^{\varphi,m}$	Lower margin of PV dispatch in scenario m
$P_{(.),t}^{\varphi,m}$	Real power output of a unit
$Q_{(.),t}^{\varphi,m}$	The reactive power output of a unit
$s_{b,t}^{(.),\varphi,m}$	Slack variables
$u_{v,t}^{\varphi,m}$	Upper margin of PV dispatch in scenario m
$PL_{l,t}^{\varphi,m}$	Real power flow in a distribution branch
$QL_{l,t}^{\varphi,m}$	Reactive power flow in a distribution branch
$SL_{l,t}^{\varphi,m}$	Apparent power flow in a distribution branch

dispatchable generation units and transmission lines. The formulated problem is solved using a decomposition technique. In [12] voltage regulators and reactive power resources are managed to maximize the hosting capacity of PV generation in the distribution network. The proposed management scheme captures the uncertainties associated with EVs in the network. A multi-objective volt/VAR control approach was presented in [13] in which a scenario-based stochastic operation scheme was used to minimize energy loss, voltage deviation, as well as total emission and energy costs. The uncertainty of renewable energy resources including solar PV generation was captured in [14] by formulating a two-stage robust optimization problem for the expansion planning of distributed generation (DG) in microgrids. The objective was to minimize the operation cost of microgrids considering the revenue for providing services to the demand entities.

The variability and uncertainty in PV generation introduce significant operation challenges including unacceptable voltage fluctuations, thermal limit violation of the distribution cables, reverse power flow, fault current measurement errors, and protection malfunctions [15]. If not addressed properly, such challenges would jeopardize the stability, reliability, and security of the distribution networks. Curtailing PV generation is considered as a practical solution to partially resolve these issues [16]; however, this solution will reduce the penetration level of PV generation and the corresponding economic and environmental benefits. Effective operation strategies such as coordinating the operation of renewable energy resources with dispatchable distributed generation technologies would improve the economic and sustainability of the distribution network operation and mitigate the adverse effects of variable and volatile PV generation in these networks [17]. A two-stage optimization model was proposed in [18], to determine the real and reactive power dispatch of controllable PV generation resources with PV power output uncertainties. A stochastic optimal voltage control strategy that captures the demand and PV generation uncertainties was proposed in [19]. A chance-constrained optimization problem was formulated to address the risk of overvoltage and voltage regulator runaway conditions in the distribution networks.

As renewable energy resources with uncertain generation patterns impose operation challenges, quantifying the extent to which such generation resources could be accommodated in power networks is crucial for the security and reliability of these systems. Dispatchable generation resources are coordinated with such variable and uncertain resources to ensure the real-time balance between the generation and demand. Therefore, the adequacy of dispatchable resources plays an important role to ensure the security of the distribution networks while mitigating renewable energy curtailments. Furthermore, determining the dispatch margins of renewable energy resources in distribution networks could be used to avoid over-investment in these resources and maximize their benefits by exploiting their installed capacity. Do-not-exceed limits for the renewable generation in power networks were quantified in [20, 21, 22]. In [20], a robust optimization problem was formulated and solved using three approaches to quantify the do-not-exceed limits for renewable generation in the bulk power network. In [21] a data-driven approach was proposed to maximize the contribution of renewable resources in the bulk power network by leveraging their do-not-exceed limits. The do-not-exceed limits are determined considering the optimal base point of the dispatchable generation units given the forecasted renewable generation. In [22] multi-period do-not-exceed limits for variable generation resources were determined considering the corrective control actions to enforce the power network constraints. While earlier research addressed the dispatch limits for renewable resources, the challenges corresponding to the integration of such variable resources in distribution networks including the unbalanced operation of the networks, the uncertainty in demand, and the risk associated with exceeding these limits require further investigation. In the authors' earlier works [23, 24], the dispatchability limits of PV generation in the unbalanced distribution network are quantified using a linear approximation of the power flow in the distribution network considering the uncertainties associated with the interconnection of electric vehicles. Furthermore, the impacts of ramp rates and energy storage on the PV dispatch margins in a distribution network with limited utility grid resources were not investigated. The contributions of this paper are as follows:

- A framework to determine the dispatch margins for PV resources in the unbalanced distribution network is proposed by formulating a mixed-integer second-order cone programming (MISOCP) problem which is solved as a two-stage problem using the column-and-constraint generation technique.
- The uncertainty in the forecasted maximum PV solar generation is captured by introducing scenarios and the uncertainty in demand is characterized by uncertainty sets.
- The impact of energy storage facilities, as well as the ramping limits of dispatchable generation resources on the PV dispatch margins in the distribution network are investigated.

The rest of the paper is organized as follows, Section 2 presents the formulated problem to determine the PV dispatch margins in the unbalanced distribution networks; Section 3 proposes the solution methodology; Section 4 presents the numerical analysis to show the effectiveness of the proposed formulation and solution approach, and Section 5 presents the conclusion.

2. Problem Formulation

Determining the PV dispatch margins could be considered as finding the largest uncertainty set for which a robust optimization problem could be solved to determine the feasible operation decisions in the distribution network. This problem is formulated as an optimization problem in which the objective is to maximize the PV generation range such

that the distribution feeder and other dispatchable generation resources could accommodate the PV generation without violating the network constraints. Here, such limits are determined considering the unbalanced generation and demand in the distribution network and the unbalanced distribution network topology. The problem formulation is shown in (1)-(32).

The objective function is shown in (1) where the objective is to expand the feasibility region for PV dispatch by maximizing the distance between the lower and upper margins while ensuring the existence of PV dispatch within these margins. Here, once $V_{v,t}^{\varphi,m} = 0$, the PV dispatch is within the upper and lower margins, and otherwise, the PV output will be outside of the dispatch margins. Therefore, minimizing $V_{v,t}^{\varphi,m}$ would accommodate the PV output between the upper and lower margins. The second term in the minimization problem is the normalized difference between the upper and lower dispatch margins of PV. The worst-case realizations of PV generation and demand are determined using the formulated max-min problem in which the slack variables that represent the mismatches in real and reactive power are minimized in (1).

The distribution network constraints are given in (2)-(9). The nodal real and reactive power balances are enforced in (2) and (3), respectively. Here, $\boldsymbol{PL}_{l,t}^{\varphi,m} \in \boldsymbol{PL}_{l,t}^{m}$, $P_{i,t}^{\varphi,m} \in \boldsymbol{PG}_{i,t}^{m}$, $P_{v,t}^{\varphi,m} \in \boldsymbol{PV}_{v,t}^{m}$, $P_{e,t}^{\varphi,m} \in \boldsymbol{PE}_{e,t}^{m}$, $P_{n,t}^{\varphi,m} \in \boldsymbol{PN}_{n,t}^{m}$, and $P_{d,t}^{\varphi,m} \in \boldsymbol{PD}_{d,t}^{m}$. Similar variables are defined for the reactive power generation and demand in the network i.e. $QL_{l,t}^{\varphi,m} \in \boldsymbol{QL}_{l,t}^{m}$, $Q_{i,t}^{\varphi,m} \in \boldsymbol{QG}_{i,t}^{m}$, $Q_{v,t}^{\varphi,m} \in \boldsymbol{QV}_{v,t}^{m}$, $Q_{e,t}^{\varphi,m} \in \boldsymbol{QE}_{e,t}^{m}$, $Q_{n,t}^{\varphi,m} \in \boldsymbol{QN}_{n,t}^{m}$, and $Q_{d,t}^{\varphi,m} \in \boldsymbol{QD}_{d,t}^{m}$. The power flow in distribution branch is formulated by (4), (5). Here, $\widetilde{\boldsymbol{R}}_l$ and $\widetilde{\boldsymbol{X}}_l$ are the resistance and inductive reactance matrices of the unbalanced branch l that are determined using the formulation presented in [25]. The big-M method is used to relax the power flow constraint once the certain phases on a distribution branch do not exist and $p_l^{\varphi} \in \mathbf{p}_l$. The relationship between the real and reactive power at the sending end of each branch is presented as (6) using a quadratic constraint which is further reformulated as a second-order cone constraint [26, 27]. Similar constraint is presented in (7) to enforce the real and reactive power capacity of the distribution feeder. The branch currents and nodal voltages are limited by (8) and (9) respectively.

The operation constraints of feeder, DG, PV generation, and energy storage system (ESS), are given in (10)-(20). The real power from the feeder is restricted by (10) and the reactive power supplied by the distribution feeder is constrained by (11)-(12) considering the acceptable power factor at the feeder. The dispatched real power of a DG unit is limited by the minimum and maximum real power capacity of the unit as enforced by (13). A similar constraint is considered for the reactive power dispatch of the unit. The power ramp for dispatchable DG units is enforced by (14). Moreover, the PV output is limited by the forecasted generation as shown in (15). The reactive power output of a PV unit is within the upper and lower acceptable limits as shown in (16). Similar constraints are considered for the real and reactive power dispatch of the ESS. The available energy in the ESS is calculated using (17) where the stored energy is within the minimum and maximum limits as enforced by (18) [28]. The available energy in the ESS at the beginning and end of the simulation period is enforced to be the same as shown in (19) and (20).

The rest of the constraints are given in (21)-(32). The lower dispatch margin is lower than the upper margin as shown in (21) and the upper margin is limited by the maximum PV capacity as shown in (22). As enforced by (23)-(24), if $V_{v,t}^{\varphi,m} = 1$, the lower and upper dispatch margins are zero. The worst-case realization of the uncertain PV generation within the polyhedral uncertainty set is determined by (25) [29]. The slack variables are positive as enforced by (26). Considering the worst-case realization of the demand would impose new constraints (27)-(32) to the problem. Here, the uncertainty in demand is captured by a polyhedral set and therefore, the real and reactive demand is represented by (27) and (28) respectively. The auxiliary binary variables used to enforce the uncertain real and reactive demands are mutually exclusive as shown in (29) and (30). The conservativeness of the solution is determined by the budget of uncertainty. Here, the budget of uncertainty is considered for the real and reactive demands using (31) and (32) respectively. As Γ_t^{φ} increases in (31), and (32) the budget of uncertainty will increase and the solution will be more conservative.

$$\min_{u_{v,t}^{\varphi,m}, l_{v,t}^{\varphi,m}, V_{v,t}^{\varphi,m}} \sum_{v,\varphi,m,t} \left[V_{v,t}^{\varphi,m} - (u_{v,t}^{\varphi,m} - l_{v,t}^{\varphi,m}) / P_{v}^{\varphi,max} \right] + \max_{\sigma_{v,t}^{\varphi,m}, \rho_{d,t}^{(.),\varphi,m}} \min_{s_{(.)}^{(.)}} \sum_{b,\varphi,m,t} \left(s_{b,t}^{1,\varphi,m} + s_{b,t}^{2,\varphi,m} + s_{b,t}^{3,\varphi,m} + s_{b,t}^{4,\varphi,m} \right) \tag{1}$$

s.t.

$$\mathbf{AL} \cdot \mathbf{PL}_{l,t}^{m} - \mathbf{AI} \cdot \mathbf{I}_{l,t}^{m} \cdot \widetilde{\mathbf{R}}_l + \mathbf{AG} \cdot \mathbf{PG}_{i,t}^{m} + \mathbf{AV} \cdot \mathbf{PV}_{v,t}^{m} + \mathbf{AE} \cdot \mathbf{PE}_{e,t}^{m} + \mathbf{AN} \cdot \mathbf{PN}_{n,t}^{m} + s_{b,t}^{1,\varphi,m} - s_{b,t}^{2,\varphi,m} = \mathbf{AD} \cdot \mathbf{PD}_{d,t}^{m} \tag{2}$$

$$\mathbf{AL}\cdot\mathbf{QL}^{m}_{l,t}-\mathbf{AI}\cdot\mathbf{I}^{m}_{l,t}\cdot\widetilde{\mathbf{X}}_{l}+\mathbf{AG}\cdot\mathbf{QG}^{m}_{i,t}+\mathbf{AV}\cdot\mathbf{QV}^{m}_{v,t}+\mathbf{AE}\cdot\mathbf{QE}^{m}_{e,t}+\mathbf{AN}\cdot\mathbf{QN}^{m}_{n,t}+s^{3,\varphi,m}_{b,t}-s^{4,\varphi,m}_{b,t}=\mathbf{AD}\cdot\mathbf{QD}^{m}_{d,t} \tag{3}$$

$$\mathbf{AL}^{\top}\cdot\mathbf{U}^{m}_{b,t}+2(\widetilde{\mathbf{R}}_{l}\cdot\mathbf{PL}^{m}_{l,t}+\widetilde{\mathbf{X}}_{l}\cdot\mathbf{QL}^{m}_{l,t})+(\widetilde{\mathbf{R}}^{2}_{l}+\widetilde{\mathbf{X}}^{2}_{l})\cdot\mathbf{I}^{m}_{l,t}\leq M\cdot(1-\mathbf{p}_{l}) \tag{4}$$

$$\mathbf{AL}^{\top}\cdot\mathbf{U}^{m}_{b,t}+2(\widetilde{\mathbf{R}}_{l}\cdot\mathbf{PL}^{m}_{l,t}+\widetilde{\mathbf{X}}_{l}\cdot\mathbf{QL}^{m}_{l,t})+(\widetilde{\mathbf{R}}^{2}_{l}+\widetilde{\mathbf{X}}^{2}_{l})\cdot\mathbf{I}^{m}_{l,t}\geq -M\cdot(1-\mathbf{p}_{l}) \tag{5}$$

$$(\mathbf{PL}^{m}_{l,t})^{2}+(\mathbf{QL}^{m}_{l,t})^{2}\leq(\mathbf{BF}\cdot\mathbf{U}^{m}_{b,t})\cdot\mathbf{I}^{m}_{l,t} \tag{6}$$

$$(\mathbf{PN}^{m}_{n,t})^{2}+(\mathbf{QN}^{m}_{n,t})^{2}\leq(\mathbf{BN}\cdot\mathbf{U}^{m}_{b,t})\cdot(\mathbf{LN}\cdot\mathbf{I}^{m}_{l,t}) \tag{7}$$

$$\mathbf{I}^{m}_{l,t}\leq\bar{\mathbf{I}}_{l} \tag{8}$$

$$\underline{\mathbf{V}}_{b}\leq\mathbf{U}^{m}_{b,t}\leq\overline{\mathbf{V}}_{b} \tag{9}$$

$$P^{\varphi,min}_{n}\leq P^{\varphi,m}_{n,t}\leq P^{\varphi,max}_{n} \tag{10}$$

$$Q^{\varphi,m}_{n,t}\leq tan\left(\cos^{-1}PF_{n}\right)\cdot P^{\varphi,m}_{n,t} \tag{11}$$

$$Q^{\varphi,m}_{n,t}\geq -tan\left(\cos^{-1}PF_{n}\right)\cdot P^{\varphi,m}_{n,t} \tag{12}$$

$$P^{\varphi,min}_{i}\leq P^{\varphi,m}_{i,t}\leq P^{\varphi,max}_{i} \tag{13}$$

$$-R_{i}\leq P^{\varphi,m}_{i,t}-P^{\varphi,m}_{i,t-1}\leq R_{i} \tag{14}$$

$$0\leq P^{\varphi,m}_{v,t}\leq P^{\varphi,f,m}_{v,t} \tag{15}$$

$$-Q^{\varphi,max}_{v}\leq Q^{\varphi,m}_{v,t}\leq Q^{\varphi,max}_{v} \tag{16}$$

$$C^{\varphi,m}_{e,t}=C^{\varphi,m}_{e,t-1}-P^{\varphi,m}_{e,t} \tag{17}$$

$$C^{\varphi,min}_{e}\leq C^{\varphi,m}_{e,t}\leq C^{\varphi,max}_{e} \tag{18}$$

$$C^{\varphi,m}_{e,0}=C^{\varphi,m}_{e,24} \tag{19}$$

$$C^{\varphi,m}_{e,0}=C^{0,\varphi,m}_{e} \tag{20}$$

$$0\leq l^{\varphi,m}_{v,t}\leq u^{\varphi,m}_{v,t} \tag{21}$$

$$u^{\varphi,m}_{v,t}\leq P^{\varphi,max}_{v} \tag{22}$$

$$\left(P^{\varphi,max}_{v}-P^{\varphi,f,m}_{v,t}\right).V^{\varphi,m}_{v,t}-l^{\varphi,m}_{v,t}\geq -P^{\varphi,f,m}_{v,t} \tag{23}$$

$$P^{\varphi,f,m}_{v,t}\cdot V^{\varphi,m}_{v,t}+u^{\varphi,m}_{v,t}\leq P^{\varphi,f,m}_{v,t} \tag{24}$$

$$P^{\varphi,m}_{v,t}=l^{\varphi,m}_{v,t}+\left(u^{\varphi,m}_{v,t}-l^{\varphi,m}_{v,t}\right).\sigma^{\varphi,m}_{v,t} \tag{25}$$

$$s^{1,\varphi,m}_{b,t},s^{2,\varphi,m}_{b,t},s^{3,\varphi,m}_{b,t},s^{4,\varphi,m}_{b,t}\geq 0 \tag{26}$$

$$P^{\varphi,m}_{d,t}=\underline{P}^{\varphi}_{d,t}\cdot\rho^{1p,\varphi,m}_{d,t}+P^{\varphi,f}_{d,t}\cdot\rho^{2p,\varphi,m}_{d,t}+\overline{P}^{\varphi}_{d,t}\cdot\rho^{3p,\varphi,m}_{d,t} \tag{27}$$

$$Q^{\varphi,m}_{d,t}=\underline{Q}^{\varphi}_{d,t}\cdot\rho^{1q,\varphi,m}_{d,t}+Q^{\varphi,f}_{d,t}\cdot\rho^{2q,\varphi,m}_{d,t}+\overline{Q}^{\varphi}_{d,t}\cdot\rho^{3q,\varphi,m}_{d,t} \tag{28}$$

$$\rho^{1p,\varphi,m}_{d,t}+\rho^{2p,\varphi,m}_{d,t}+\rho^{3p,\varphi,m}_{d,t}=1 \tag{29}$$

$$\rho^{1q,\varphi,m}_{d,t}+\rho^{2q,\varphi,m}_{d,t}+\rho^{3q,\varphi,m}_{d,t}=1 \tag{30}$$

$$\sum_{d}(\rho^{1p,\varphi,m}_{d,t}+\rho^{3p,\varphi,m}_{d,t})\leq\Gamma^{\varphi}_{t} \tag{31}$$

$$\sum_{d}(\rho^{1q,\varphi,m}_{d,t}+\rho^{3q,\varphi,m}_{d,t})\leq\Gamma^{\varphi}_{t} \tag{32}$$

3. Solution Methodology

The compact form of the problem formulation is presented in (33)-(38) as follows:

$$\min_{\boldsymbol{x}} \ \boldsymbol{c}^{\top}\boldsymbol{x} + \max_{\boldsymbol{\xi}} \ \min_{\boldsymbol{y}} \ \boldsymbol{b}^{\top}\boldsymbol{y} \tag{33}$$

s.t.

$$\boldsymbol{A}\boldsymbol{x} \leq \boldsymbol{d} \tag{34}$$

$$\boldsymbol{F}\boldsymbol{x} + \boldsymbol{Q}\boldsymbol{y} + (\boldsymbol{D}\cdot\boldsymbol{x})^{\top}\boldsymbol{\xi} + \boldsymbol{M}\boldsymbol{\xi} = \boldsymbol{h} \tag{35}$$

$$\boldsymbol{E}\boldsymbol{y} \leq \boldsymbol{g} \tag{36}$$

$$\|\boldsymbol{G}\boldsymbol{y}\|_2 \leq \boldsymbol{m}^{\top}\boldsymbol{y} \tag{37}$$

$$\boldsymbol{L}\boldsymbol{\xi} \leq \boldsymbol{w} \tag{38}$$

The problem is reformulated as a two-stage robust optimization problem, where $\boldsymbol{x}$ is the vector of first-stage decision variables i.e. $\left[l_{v,t}^{\varphi,m}, u_{v,t}^{\varphi,m}, V_{v,t}^{\varphi,m}\right]$ and $\boldsymbol{y}$ is the vector of second-stage recourse decision variables i.e. $P_{v,t}^{\varphi,m}$, $P_{e,t}^{\varphi,m}$, $P_{n,t}^{\varphi,m}$, $P_{i,t}^{\varphi,m}$, $Q_{v,t}^{\varphi,m}$, $Q_{n,t}^{\varphi,m}$, $Q_{i,t}^{\varphi,m}$, $PL_{l,t}^{\varphi,m}$, $QL_{l,t}^{\varphi,m}$ and $s_{b,t}^{(.),\varphi,m}$ as well as the voltage magnitude on the buses ($\boldsymbol{U}_{b,t}^{m}$). Here, $\boldsymbol{\xi}$ is a vector representing the uncertain variables where $\rho_{d,t}^{(.),\varphi,m} \in \boldsymbol{\xi}$ and $\sigma_{v,t}^{\varphi,m} \in \boldsymbol{\xi}$. The constraint (34) represents (21)-(24); constraint (35) represents the set of constraints (2)-(3), (25), (27) and (28). Constraint (37) represents constraints (6)-(7). Constraints (38), represents constraints (29)-(32). The rest of the constraints are represented by constraint (36).

The proposed solution approach is based on the column-and-constraint generation algorithm presented in [30]. The flowchart of the proposed solution methodology is shown in Fig. 1. As shown in this figure, in the master problem (first stage), the upper and lower margins of PV generation are determined by maximizing the difference between the upper and lower margins, using the normalized term $(u_{v,t}^{\varphi,m} - l_{v,t}^{\varphi,m})/P_{v}^{\varphi,max}$ in the objective function. By solving the subproblem at the second stage, the operation decisions considering the worst-case realization of the uncertain variables are determined. The solution procedure is presented in the following steps.

1) Step 1 – Initialize the iteration count at $k = 0$ and the convergence threshold at $\varepsilon_1 \leq 10^{-3}$. Set the $LB = -\infty$ and $UB = \infty$.

2) Step 2 – Solve the master problem with the objective function shown in (39) and the constraints (40)-(44). Determine the solution for $l_{v,t}^{\varphi,m}, u_{v,t}^{\varphi,m}, V_{v,t}^{\varphi,m}$ by fixing the solution obtained from the subproblem (e.g. ξ^*). The upper and lower margins of the PV generation determined in the master problem ($\boldsymbol{x}^*$) are passed to the subproblem.

$$\min_{\boldsymbol{x}} \ \boldsymbol{c}^{\top}\boldsymbol{x} + \eta \tag{39}$$

s.t.

$$\boldsymbol{A}\boldsymbol{x} \leq \boldsymbol{d} \tag{40}$$

$$\eta \geq \boldsymbol{b}^{\top}\boldsymbol{y}^{l}; \forall l \leq k \tag{41}$$

$$\boldsymbol{F}\boldsymbol{x} + \boldsymbol{Q}\boldsymbol{y}^{l} + (\boldsymbol{D}\cdot\boldsymbol{x})^{\top}\boldsymbol{\xi}^{*} + \boldsymbol{M}\boldsymbol{\xi}^{*} = \boldsymbol{h}; \forall l \leq k \tag{42}$$

$$\boldsymbol{E}\boldsymbol{y}^{l} \leq \boldsymbol{g}; \forall l \leq k \tag{43}$$

$$\left\|\boldsymbol{G}\boldsymbol{y}^{l}\right\|_2 \leq \boldsymbol{m}^{\top}\boldsymbol{y}^{l}; \forall l \leq k \tag{44}$$

Update the LB using (45):

$$LB = \boldsymbol{c}^{\top}\boldsymbol{x}^{*} + \hat{\eta}_{k+1} \tag{45}$$

3) Step 3 –Solve the subproblem with the objective function in (46) and constraints (47)-(50).

$$\max_{\xi} \min_{y} \ \boldsymbol{b}^{\top}\boldsymbol{y} \tag{46}$$

$$\text{s.t.} \quad \boldsymbol{Q}\boldsymbol{y} = \boldsymbol{h} - (\boldsymbol{D}\cdot\boldsymbol{x}^{*})^{\top}\boldsymbol{\xi} - \boldsymbol{M}\boldsymbol{\xi} - \boldsymbol{F}\boldsymbol{x}^{*} \quad : \boldsymbol{\mu}_1 \tag{47}$$

$$\boldsymbol{E}\boldsymbol{y} \le \boldsymbol{g} \qquad : \boldsymbol{\mu}_2 \tag{48}$$

$$\|\boldsymbol{G}\boldsymbol{y}\|_2 \le \boldsymbol{m}^{\top}\boldsymbol{y} \qquad : \boldsymbol{\mu}_3, \boldsymbol{\mu}_4 \tag{49}$$

$$\boldsymbol{L}\boldsymbol{\xi} \le \boldsymbol{w} \tag{50}$$

Here, the subproblem (46)-(50) is reformulated as (51)-(55) using the duality theory.

$$\psi(\boldsymbol{y}) = \max_{\xi} \left[\boldsymbol{h} - (\boldsymbol{D}\cdot\boldsymbol{x}^{*})^{\top}\boldsymbol{\xi} - \boldsymbol{M}\boldsymbol{\xi} - \boldsymbol{F}\boldsymbol{x}^{*}\right]^{\top}\boldsymbol{\mu}_1 + \boldsymbol{g}^{\top}\boldsymbol{\mu}_2 \tag{51}$$

$$\text{s.t.} \quad \boldsymbol{Q}^{\top}\boldsymbol{\mu}_1 + \boldsymbol{E}^{\top}\boldsymbol{\mu}_2 \le \boldsymbol{b} \tag{52}$$

$$\left\|\boldsymbol{\mu}_3\right\|_2 \le \boldsymbol{\mu}_4 \tag{53}$$

$$\boldsymbol{L}\boldsymbol{\xi} \le \boldsymbol{w} \tag{54}$$

$$\boldsymbol{\mu}_2 \le 0, \quad \boldsymbol{\mu}_1 \quad free \tag{55}$$

The nonlinear term $\boldsymbol{\mu}_1\boldsymbol{\xi}$ in (51) is linearized using McCormick envelopes. Considering $\boldsymbol{\upsilon} = \boldsymbol{\mu}_1\boldsymbol{\xi}$, the nonlinear term $\boldsymbol{\upsilon}$ is linearized by (56)-(59) [31].

$$\boldsymbol{\upsilon} \ge \underline{\boldsymbol{\mu}}_1\boldsymbol{\xi} + \boldsymbol{\mu}_1\underline{\boldsymbol{\xi}} - \underline{\boldsymbol{\mu}}_1\underline{\boldsymbol{\xi}} \tag{56}$$

$$\boldsymbol{\upsilon} \ge \overline{\boldsymbol{\mu}}_1\boldsymbol{\xi} + \boldsymbol{\mu}_1\overline{\boldsymbol{\xi}} - \overline{\boldsymbol{\mu}}_1\overline{\boldsymbol{\xi}} \tag{57}$$

$$\boldsymbol{\upsilon} \le \overline{\boldsymbol{\mu}}_1\boldsymbol{\xi} + \boldsymbol{\mu}_1\underline{\boldsymbol{\xi}} - \overline{\boldsymbol{\mu}}_1\underline{\boldsymbol{\xi}} \tag{58}$$

$$\boldsymbol{\upsilon} \le \boldsymbol{\mu}_1\overline{\boldsymbol{\xi}} + \underline{\boldsymbol{\mu}}_1\boldsymbol{\xi} - \underline{\boldsymbol{\mu}}_1\overline{\boldsymbol{\xi}} \tag{59}$$

Update the upper bound of the solution using (60) and go to *Step 4*.

$$UB = min\{UB, \boldsymbol{c}^{\top}\boldsymbol{x}^{*(k+1)} + \psi(\boldsymbol{y}^{*(k+1)})\} \tag{60}$$

4) Step 4 – Check if $UB - LB \le \varepsilon_1$. If this condition is satisfied, terminate the procedure; otherwise, go to *Step 5*.
5) Step 5 – Generate the columns and constraints by creating additional decision variables and adding constraint (41)-(44). Set $k = k + 1$ and go to *Step 2*.

4. Numerical Results

In this section, the modified IEEE-13 bus system is considered as a test case. The simulations are performed on a PC with Intel 3.4 GHz Core i5 processor and 8 GB memory, using MOSEK solver. The diagram of the modified IEEE 13-bus system is shown in Fig. 2 and the characteristics of dispatchable DG and PV units are shown in Tables 1 and 2 respectively. All DG units except DG4 are three-phase units. DG4 is a single-phase unit installed on phase C. The total peak real power demand on phases A, B, and C are 1175 kW, 1039 kW, and 1252 kW respectively. The total peak reactive power demand on phases A, B, and C are 616 kVAr, 665 kVAr, and 771 kVAr respectively. Fig. 3 shows the demand profile and the total PV generation in the operation horizon. The forecasted PV generation is determined based on the solar radiation for location ID 883549 on 8/9/2017 from [32]. The approximated feeder capacity is 2800 kW with the least acceptable power factor of 0.82. The dispatch margins of PV generation in the three-phase unbalanced system are evaluated in Cases 1-3 and the impacts of ramping limits of DG units and ESS on the dispatch margins of PV generation are evaluated in Case 4.
Case 1 – PV dispatch margins with forecasted maximum PV generation and demand.
Case 2 – PV dispatch margins with forecasted maximum PV generation and worst-case realization of demand.
Case 3 – PV dispatch margins with uncertain maximum PV generation and uncertain demand.
Case 4 - Operation in island mode with the loss of the main feeder

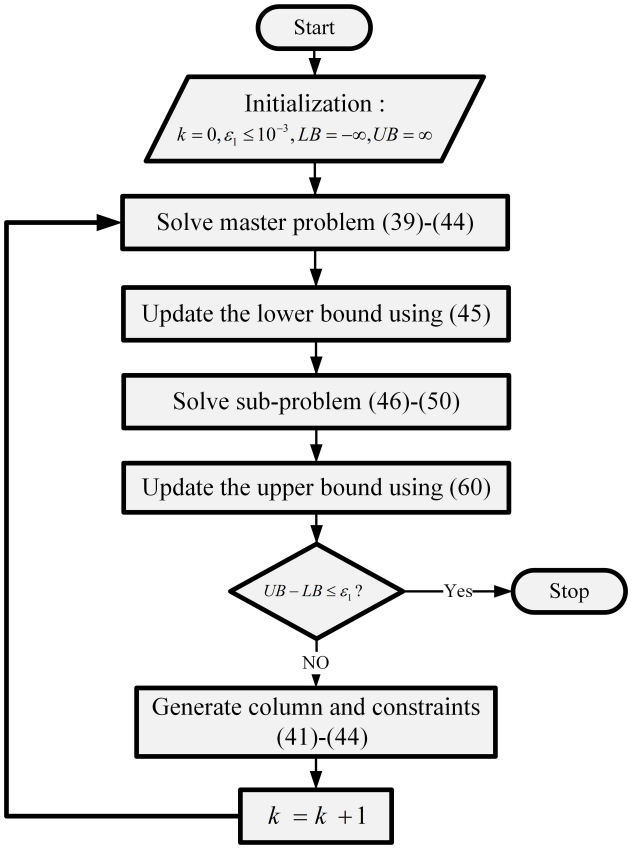

Figure 1: The proposed solution algorithm

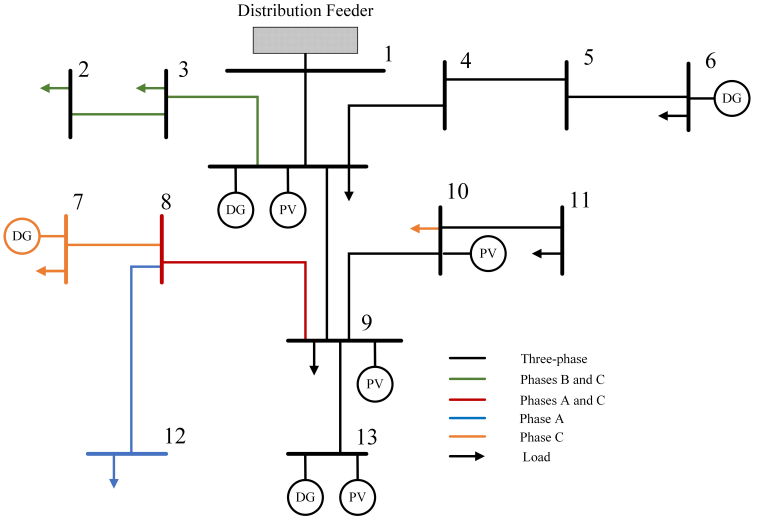

Figure 2: The modified IEEE 13-bus distribution network.

4.1. Case1 – PV dispatch margins with forecasted maximum PV generation and demand

In this case, the demand and maximum PV generation follow the respective forecasted profiles. The dispatch margins of PV generation on phase C are shown in Fig. 4. Here, the lower dispatch margin of PV generation on phase C is

Table 1
Dispatchable DG Units' Characteristics

DG	Bus	P^{min}	P^{max}	Q^{min}	Q^{max}
1	4	0	200	-100	100
2	6	0	200	-100	100
3	13	0	250	-120	120
4	7	0	40	-20	20

Table 2
PV Generation Units' Characteristics

PV	Bus	P^{min}	P^{max}	Q^{min}	Q^{max}
1	13	0	200	-100	100
2	10	0	200	-100	100
3	9	0	200	-100	100
4	4	0	100	-50	50

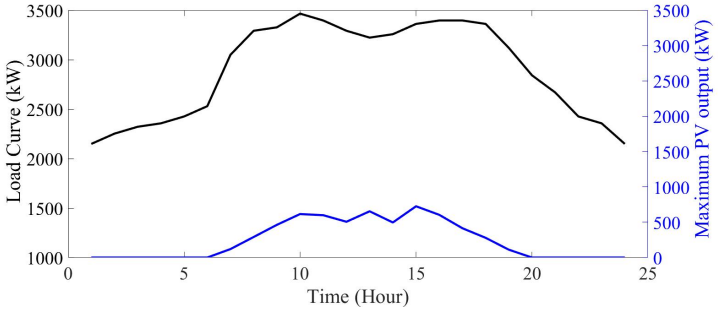

Figure 3: Daily profile of demand and maximum PV generation.

increased from 11.018 kW at hour 8, to 23.585 kW and 73.917 kW at hours 9 and 10 respectively. Similarly, the lower dispatch margin of PV generation is increased from 36.182 kW at hour 15, to 48.752 kW at hours 16 and 17. At hour 10, the demand on phase C is 1252 kW, and the total output of the feeder and DG units is 1229.094 kW. The power loss at this hour is 51.094 kW and therefore, the total power loss and demand at this hour is 1303.094 kW. Decreasing the dispatch of PV generation will result in the increase in the dispatch of DG units and the main feeder; however, the total dispatch of DG units and the main feeder cannot exceed 1229.094 kW as they reach their maximum power capacities. Therefore, the lower PV dispatch margin at hour 10 on phase C is 73.917 kW. Similarly, at hour 11, the demand on phase C is 1226.9 kW and the total output power of the feeder and DG units is 1230.848 kW. At this hour the power loss is 52.640 kW and therefore, the total power loss and demand reaches 1279.6 kW. The lower dispatch margin of PV generation on phase C at this hour is 48.752 kW. In this case, the lower dispatch margins on phase B are zero at all hours.

4.2. Case 2 – PV dispatch margins with forecasted maximum PV generation and worst-case realization of demand

In this case, the uncertainty set for demand is within 0.95 and 1.05 of the forecasted values. The upper and lower margins for PV generations were determined considering the worst-case realization of demand within the uncertainty set. The budget of uncertainty is defined as the portion of demand entities that have the flexibility to variate within the uncertainty set. If the budget of uncertainty is 0%, the demand equals the forecasted value. When the budget of uncertainty is increased to 100%, the demand on all phases at all buses could vary between the possible minimum and maximum values represented by the uncertainty set. The PV dispatch margins on phase C considering the forecasted demand as well as the worst-case realization of the demand are shown in Fig. 4. In Fig. 4, it is shown that when the

budget of uncertainty is 100%, the lower PV dispatch margin increases. In Fig. 4, with 100% budget of uncertainty, at hour 10, the demand in the distribution network is 1306.10 kW, the power loss is 12.173 kW and the outputs of the feeder and DG are at their maximum and their total output reaches 1189.99 kW. Therefore, at this hour, the rest of the demand is supplied by the PV units, and the lower margin of PV dispatch increases to 128.282 kW.

The upper margins for PV generation in Case 1 and Case 2 are the same. In Case 2, the lower margins at hours 17 and 18 are 101.907 kW and 89.008 kW respectively. At hour 18, the difference between the lower and upper margins reaches 4.043 kW as the PV generation decreases and the demand reaches 1266.917 kW.

In this case, the maximum PV generation is the same for all phases; however, the demand on phase C is larger than that on the other two phases; therefore, the lower PV dispatch margin on phase C is higher than that on the other phases. Here, the PV generation on phase C is dispatched to serve the demand if the power capacities of the feeder and distributed generation are not adequate to serve the demand on this phase. The dispatch margins for PV generation units on phase C are shown in Fig. 5. As shown in this figure, at hour 10, both the minimum and maximum dispatch margin for PV2 and PV3 are 58.538 kW, which indicates that at this hour, the generation unit of PV3 has to be fully dispatched to serve the demand.

The uncertainty in demand will increase the lower PV dispatch margin. Fig. 6 shows the difference between the upper and lower margins of the total PV generation as the budget of uncertainty varies from 0% to 100%. As shown in Fig. 6, as the budget of uncertainty increases, the difference between the upper and lower dispatch margins will decrease. With a 100% budget of uncertainty, at hour 13, the total real demand of 3376.645 kW and the total loss of 120.484 kW are supplied by the main distribution feeder, DG units and PV generation units. The main distribution feeder and DG units supply 3300.989 kW and the PV generation units serve 196.14 kW.

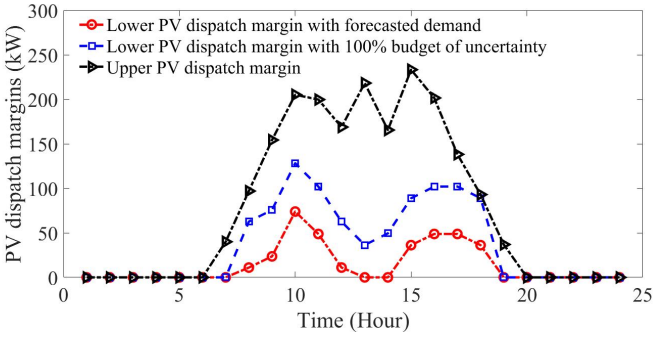

Figure 4: The total dispatch margins on phase C with forecasted demand (Case 1) and the worst-case realization of demand with 100% budget uncertainty (Case 2).

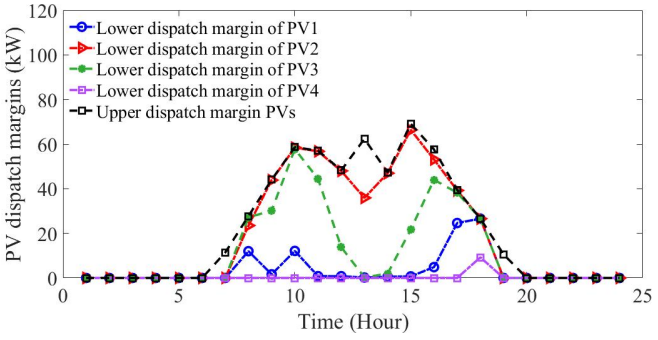

Figure 5: The dispatch margins of PV generation units on phase C (Case 2)

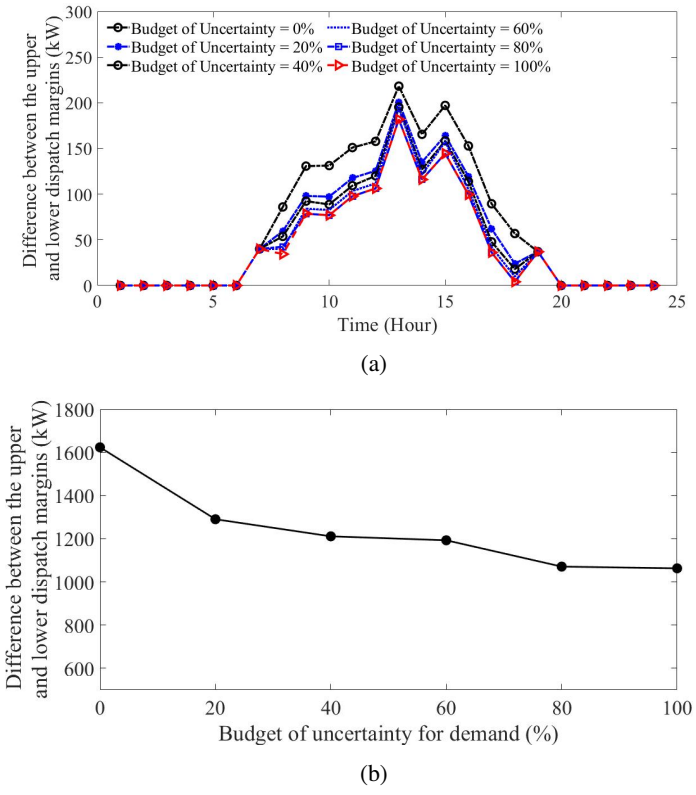

Figure 6: The difference between the upper and lower PV dispatch margins for different budgets of uncertainty in demand (a) total hourly difference (b) total day-ahead difference.

4.3. Case 3 – PV dispatch margins with uncertain maximum PV generation and demand

Here, the Gaussian probability distribution function is used to represent the forecast errors in the maximum PV generation and demand, and Monte-Carlo simulation is used to generate 100 scenarios. The mean of the probability distribution function is the forecasted values in Cases 1 and 2, and the standard deviation is 0.025 of the mean values. The total upper and lower PV dispatch margins on phase C in 5 scenarios and the expected upper and lower dispatch margins are shown in Fig. 7. In Fig. 8, the expected upper and lower PV dispatch margins are compared with those procured in Case 1. As shown in this figure, the lower PV dispatch margin, in this case, is higher than that in Case 1. Here, the lower and upper dispatch margins (i.e., $\tilde{u}^{\varphi}_{v,t}$ and $\tilde{l}^{\varphi}_{v,t}$), are determined in a way that the risk of violating these margins are constrained as shown in (61) and (62). Fig. 7 shows the upper and lower margins for which the probability of exceeding these margins does not exceed 10%. Here, the upper and lower dispatch margins are determined so that such limits do not violate in more than 10% of scenarios. Fig. 8 shows the procured risk-based upper and lower dispatch margins (i.e. $\tilde{u}^{\varphi}_{v,t}$ and $\tilde{l}^{\varphi}_{v,t}$) compared to those procured in Case 1, and the expected lower and upper dispatch margins for 100 scenarios in this case. Table 3, shows the total lower and upper dispatch limits of PV generation once the probability of exceeding such limits is increased from 5% to 50%. As shown in this table, as the probability of violating the upper and lower bounds increases, the risk-based upper margin decreases while the risk-based lower margin increases.

Once the uncertainty in demand is represented by polyhedral sets with 100% budget of uncertainty, the expected upper and lower dispatch margins for phases A, B, and C are shown in Fig. 9. Here, the total expected upper dispatch margins on all phases are 1956.4 kWh which is equal to the expected upper dispatch margin of PV generation with scenario-based demand. Furthermore, similar to the case with scenario-based demand, the total expected lower dispatch margin on phase B is zero, as the demand on phase B can be supplied by the feeder and DGs. The total expected lower dispatch margins on phases A and C are 558.59 kWh and 891.77 kWh, respectively. These margins are higher than the total expected lower dispatch margins with scenario-based demand on these phases, i.e. 125.85 kWh for phase A, and

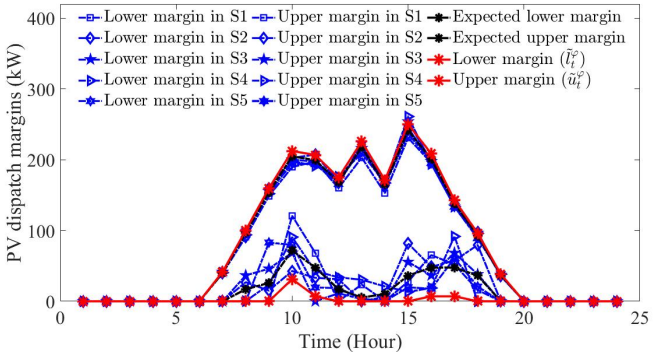

Figure 7: The total PV dispatch margins on phase C in five scenarios S1-S5, the expected PV dispatch margins, and the risk-based upper and lower dispatch margins for $\varepsilon = 0.1$ in Case 3

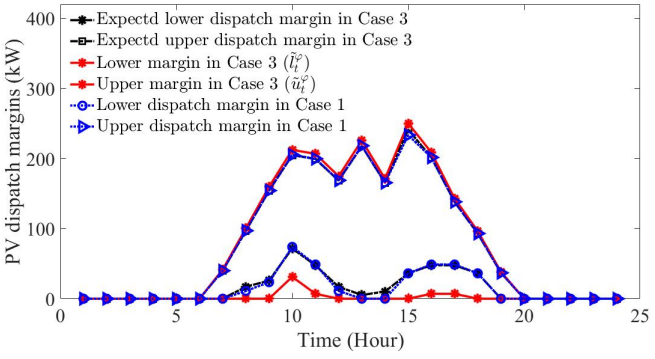

Figure 8: The expected upper and lower PV dispatch margins in Case 1 and Case 3 and the risk-based upper and lower dispatch margins with $\varepsilon = 0.1$

Table 3
The total risk-based lower and upper dispatch margins of PV generation units on phase C in 24 hours

ε	Total Lower Dispatch Margin (kWh)	Total Upper Dispatch Margin (kWh)
0.05	17.47	2034.65
0.1	52.42	2028.16
0.2	113.22	2001.94
0.3	200.52	1987.62
0.4	237.54	1972.41
0.5	307.19	1956.04

362.17 kWh for phase C.

$$\mathbb{P}\left[\hat{u}_{v,t}^{\varphi,m} \leq \tilde{u}_{v,t}^{\varphi}\right] \geq 1-\varepsilon \tag{61}$$

$$\mathbb{P}\left[\hat{l}_{v,t}^{\varphi,m} \geq \tilde{l}_{v,t}^{\varphi}\right] \geq 1-\varepsilon \tag{62}$$

4.4. Case 4 – Operation in island mode with the loss of the main feeder

In this case, the main feeder is disconnected and the distribution network is supplied by the DG and PV generation units. The characteristics of the DG units are shown in Table 4. As shown in Fig. 10a, at hour 10, the peak demand on

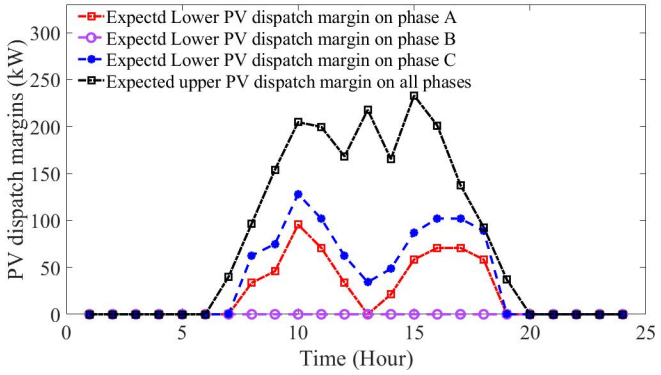

Figure 9: The expected dispatch margins of PV generation units on phases A, B and C with uncertain PV generation and worst-case realization of demand

Table 4
Characteristics of dispatchable DG units in the islanded mode operation of the IEEE-13 bus system.

DG	Bus	Ramp Rate (kW/hr)	P^{max} (kW)	Q^{min} (kVar)	Q^{max} (kVar)
1	4	225	1010	-505	505
2	6	225	1010	-505	505
3	13	240	1260	-700	700
4	7	15	60	-30	30

Table 5
Characteristics of ESS in the island mode operation of the IEEE-13 bus system.

ESS	Bus	P^{max}	Q^{max}	E^{min}	E^{max}
1	4	200	120	0	200
2	10	200	120	0	200

phase A is 1175 kW and the power loss is 47.551 kW. The total generation of DG units is 1137.562 kW.Therefore, the rest of the demand is served by the PV generation and the lower PV dispatch margin is $1175+47.551-1137.562 = 84.989$ kW. Similarly, in Fig. 10b, on phase C, the total demand is 1252 kW and the power loss is 44.025 kW and the total generation of DG units is 1195.02 kW, therefore the rest of the demand i.e. $1252 + 44.025 - 1195.02 = 101.658$ kW is supplied by the PV generation and the lower PV dispatch margin is 101.658 kW. Furthermore, Fig. 10 demonstrates the effect of ramp rates on the PV dispatch margins. As shown in Fig. 10a, when ramp rates are not considered, the lower PV dispatch margins on phase A at hours 12, 16, are 0 kW. By considering the ramp rates for DG units as shown in Table 4, the lower PV dispatch margins at hours 12, and 16 are increased to 26.199 kW, and 61.481 kW respectively. Furthermore, the impact of ESSs on the PV dispatch margins are shown in Fig. 10. The characteristics of ESSs considered, in this case, are shown in Table 5. As shown in Fig. 10a, the lower PV dispatch margin on phase A is dramatically reduced after installing the ESSs. Here, the lower PV dispatch margins are decreased from 84.989 kW, and 101.658 kW at hour 10, to 0.340 kW and 26.221 kW on phases A, and C respectively.
Considering the ramp rates for DG units will decrease the difference between the lower and upper PV dispatch margins. In the day-ahead operation horizon, the total difference between the upper and lower PV dispatch margins in the island operation mode of the distribution network ignoring the ramp rates of DG units are 1580.35 kWh, 1951.877 kWh, and 1580.35 kWh on phases A, B, and C, respectively. Once ramp rates are considered, such values are reduced to 1478.23 kWh, 1951.877 kWh, and 1336.185 kWh for phases A, B, and C, respectively. Furthermore, utilizing the

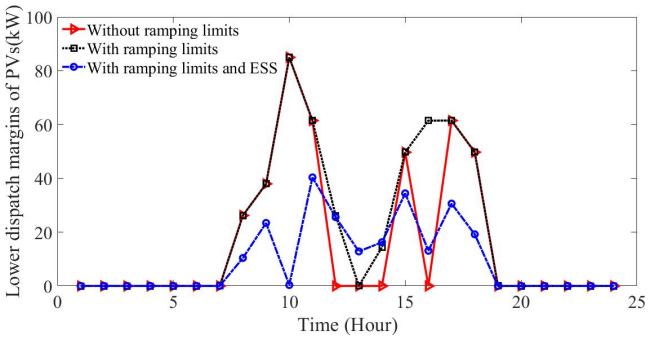

(a)

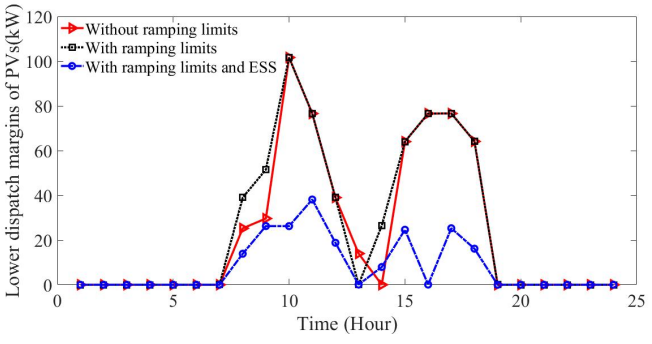

(b)

Figure 10: The lower PV dispatch margin on (a) phase A and (b) phase C for isolated distribution network considering the ramp rate for DG units and energy storage.

ESSs will increase the difference between the upper and lower PV dispatch margins. Here, integrating ESS with ramp rates of DG units will increase the total difference between the upper and lower dispatch margins in the day-ahead operation horizon to 1725.421 kWh, 1951.887 kWh and 1754.519 kWh on phases A, B, and C, respectively.

5. Conclusion

In this paper, the upper and lower PV dispatch margins in unbalanced three-phase distribution systems are determined to ensure the security of the distribution network. A two-stage optimization problem is formulated and a solution approach is proposed to solve this problem. The modified IEEE 13-bus system is used to evaluate the effectiveness of the proposed formulation and solution methodology. It is shown that the worst-case realization of demand will increase the lower PV dispatch margins and decreases the difference between the lower and upper PV dispatch margins. Furthermore, increasing the budget of uncertainty for demand will decrease the difference between the lower and upper PV dispatch margins. The uncertainty in maximum PV generation and demand is considered using scenarios. Compared to the scenario-based models that address the uncertainty in demand, it is shown that the lower PV dispatch margins are higher once the worst-case realization of demand is considered. Furthermore, the risk associated with violating the upper and lower dispatch margins is considered. The impacts of the ramp rates of DG units and the installation of ESSs on the PV dispatch margins are investigated. It is shown that imposing the ramp rates for the DG units will increase the lower PV dispatch margins and leveraging ESSs increases the difference between the lower and upper PV dispatch margins and decreases the lower PV dispatch margins.

References

[1] W. Warwick, T. Hardy, M. Hoffman, J. Homer, Electricity distribution system baseline report, Pacific Northwest National Laboratory, Tech Rep PNNL 25178 (2016).

[2] U. S., EIA, Annual energy outlook 2019 with projections to 2050 (2019).

[3] R. Torquato, D. Salles, C. O. Pereira, P. C. M. Meira, W. Freitas, A comprehensive assessment of pv hosting capacity on low-voltage distribution systems, IEEE Transactions on Power Delivery 33 (2018) 1002–1012.

[4] D. Zhu, A. K. Jain, R. Broadwater, F. Bruna, Feeder voltage profile design for energy conservation and pv hosting capacity enhancement, Electric Power Systems Research 164 (2018) 263–271.

[5] F. Ding, B. Mather, On distributed pv hosting capacity estimation, sensitivity study, and improvement, IEEE Transactions on Sustainable Energy 8 (2016) 1010–1020.

[6] D. Chathurangi, U. Jayatunga, S. Perera, A. Agalgaonkar, T. Siyambalapitiya, A nomographic tool to assess solar pv hosting capacity constrained by voltage rise in low-voltage distribution networks, International Journal of Electrical Power & Energy Systems 134 (2022) 107409.

[7] S. Hashemi, J. Østergaard, Efficient control of energy storage for increasing the pv hosting capacity of lv grids, IEEE Transactions on Smart Grid 9 (2016) 2295–2303.

[8] S. Hashemi, J. Østergaard, T. Degner, R. Brandl, W. Heckmann, Efficient control of active transformers for increasing the pv hosting capacity of lv grids, IEEE Transactions on Industrial Informatics 13 (2016) 270–277.

[9] A. Dubey, S. Santoso, On estimation and sensitivity analysis of distribution circuit's photovoltaic hosting capacity, IEEE Transactions on Power Systems 32 (2016) 2779–2789.

[10] X. Xu, J. Li, Z. Xu, J. Zhao, C. S. Lai, Enhancing photovoltaic hosting capacity—a stochastic approach to optimal planning of static var compensator devices in distribution networks, Applied energy 238 (2019) 952–962.

[11] M. Alanazi, M. Mahoor, A. Khodaei, Co-optimization generation and transmission planning for maximizing large-scale solar pv integration, International Journal of Electrical Power & Energy Systems 118 (2020) 105723.

[12] A. Ali, K. Mahmoud, M. Lehtonen, Maximizing hosting capacity of uncertain photovoltaics by coordinated management of oltc, var sources and stochastic evs, International Journal of Electrical Power & Energy Systems 127 (2021) 106627.

[13] T. Niknam, M. Zare, J. Aghaei, Scenario-based multiobjective volt/var control in distribution networks including renewable energy sources, IEEE Transactions on Power Delivery 27 (2012) 2004–2019.

[14] Z. Wang, B. Chen, J. Wang, J. Kim, M. M. Begovic, Robust optimization based optimal dg placement in microgrids, IEEE Transactions on Smart Grid 5 (2014) 2173–2182.

[15] R. Seguin, J. Woyak, D. Costyk, J. Hambrick, B. Mather, High-penetration PV integration handbook for distribution engineers, Technical Report, National Renewable Energy Lab.(NREL), Golden, CO (United States), 2016.

[16] L. Bird, J. Cochran, X. Wang, Wind and solar energy curtailment: Experience and practices in the United States, Technical Report, National Renewable Energy Lab.(NREL), Golden, CO (United States), 2014.

[17] A. Mills, Understanding variability and uncertainty of photovoltaics for integration with the electric power system (2009).

[18] T. Ding, C. Li, Y. Yang, J. Jiang, Z. Bie, F. Blaabjerg, A two-stage robust optimization for centralized-optimal dispatch of photovoltaic inverters in active distribution networks, IEEE Transactions on Sustainable Energy 8 (2016) 744–754.

[19] Y. P. Agalgaonkar, B. C. Pal, R. A. Jabr, Stochastic distribution system operation considering voltage regulation risks in the presence of pv generation, IEEE Transactions on Sustainable Energy 6 (2015) 1315–1324.

[20] J. Zhao, T. Zheng, E. Litvinov, Variable resource dispatch through do-not-exceed limit, IEEE Transactions on Power Systems 30 (2014) 820–828.

[21] Z. Li, F. Qiu, J. Wang, Data-driven real-time power dispatch for maximizing variable renewable generation, Applied energy 170 (2016) 304–313.

[22] Z. Li, F. Qiu, J. Wang, Multi-period do-not-exceed limit for variable renewable generation dispatch considering discrete recourse controls, arXiv preprint arXiv:1608.05273 (2016).

[23] M. R. Feizi, M. Khodayar, B. Chen, Feasible dispatch limits of pv generation with uncertain interconnection of evs in the unbalanced distribution network, IEEE Transactions on Vehicular Technology (2021).

[24] M. R. Feizi, M. E. Khodayar, Dispatchability limits for pv generation in unbalanced distribution networks with evs, in: 2020 IEEE Power & Energy Society General Meeting (PESGM), IEEE, 2020, pp. 1–5.

[25] B. Chen, C. Chen, J. Wang, K. L. Butler-Purry, Sequential service restoration for unbalanced distribution systems and microgrids, IEEE Transactions on Power Systems 33 (2017) 1507–1520.

[26] S. R. Shukla, S. Paudyal, M. R. Almassalkhi, Efficient distribution system optimal power flow with discrete control of load tap changers, IEEE Transactions on Power Systems 34 (2019) 2970–2979.

[27] H. Ji, C. Wang, P. Li, J. Zhao, G. Song, F. Ding, J. Wu, An enhanced socp-based method for feeder load balancing using the multi-terminal soft open point in active distribution networks, Applied Energy 208 (2017) 986–995.

[28] Y. Zheng, J. Zhao, Y. Song, F. Luo, K. Meng, J. Qiu, D. J. Hill, Optimal operation of battery energy storage system considering distribution system uncertainty, IEEE Transactions on Sustainable Energy 9 (2017) 1051–1060.

[29] A. Thiele, T. Terry, M. Epelman, Robust linear optimization with recourse, Rapport technique (2009) 4–37.

[30] B. Zeng, L. Zhao, Solving two-stage robust optimization problems using a column-and-constraint generation method, Operations Research Letters 41 (2013) 457–461.

[31] A. Mitsos, B. Chachuat, P. I. Barton, Mccormick-based relaxations of algorithms, SIAM Journal on Optimization 20 (2009) 573–601.

[32] Nrel nsrdb data viewer, access 10/11/2021. URL: https://maps.nrel.gov/nsrdb-viewer/.